

Computer simulation of three-dimensional heavy ion beam trajectory imaging techniques used for magnetic field estimation

C. Ling, K. A. Connor, D. R. Demers, R. J. Radke, and P. M. Schoch^{a)}
 ECSE Department, Rensselaer Polytechnic Institute, Troy, New York, 12180, USA

(Received 28 August 2007; accepted 6 October 2007; published online 26 November 2007)

A magnetic field mapping technique via heavy ion beam trajectory imaging is being developed on the Madison Symmetric Torus reversed field pinch. This paper describes the computational tools created to model camera images of the light emitted from a simulated ion beam, reconstruct a three-dimensional trajectory, and estimate the accuracy of the reconstruction. First, a computer model is used to create images of the torus interior from any candidate camera location. It is used to explore the visual field of the camera and thus to guide camera parameters and placement. Second, it is shown that a three-dimensional ion beam trajectory can be recovered from a pair of perspectively projected trajectory images. The reconstruction considers effects due to finite beam size, nonuniform beam current density, and image background noise. Third, it is demonstrated that the trajectory reconstructed from camera images can help compute magnetic field profiles, and might be used as an additional constraint to an equilibrium reconstruction code, such as MSTFit.

© 2007 American Institute of Physics. [DOI: [10.1063/1.2804108](https://doi.org/10.1063/1.2804108)]

I. INTRODUCTION

This paper presents several computational tools required for processing images of a heavy ion beam and estimating the magnetic field within a plasma. The concept, first proposed by Jobes and Peng,¹ uses emission from an ion beam (which is deflected by a confining magnetic field) to reconstruct the magnetic field. Imaging the emission of the electron-impact-excited ions renders the trajectory of the beam throughout the plasma which yields a measure of the magnetic field component perpendicular to the beam velocity. The reconstructed trajectory can also be used as a constraint within magnetic profile reconstruction methods. Demers *et al.*^{2,3} have previously investigated several issues including ion beam current density optimization and the selection of wavelengths suitable for spectroscopic measurements of primary ion beam emission.

The computer modeling throughout this paper uses simulated ion beam trajectory images and assumes that emission from the beam is sufficiently bright to be captured by charge coupled device cameras. This simulation is modeled after operation of the HIBP installed on the Madison Symmetric Torus (MST) reversed field pinch (RFP).⁴ In a RFP device, the magnetic fields are predominantly generated by currents in the plasma that are not known *a priori*. Therefore, this technique may help determine the equilibrium magnetic field. We propose to incorporate reconstructed ion beam trajectory data as an additional constraint to the MSTFit code⁵ which computes the equilibrium by finding the best fit to the Grad-Shafranov equation.

The contributions of this paper are threefold. First, we describe a computer simulation of MST that is used to gen-

erate synthetic experimental images. Second, we demonstrate how two images of the ion beam trajectory inside the torus interior are used to reconstruct the three-dimensional trajectory, given sufficient information about camera placement. The simulated images take into consideration finite beam size and current density distribution as well as background noise. Third, we show that under reasonable image noise conditions, the estimated error in the reconstructed trajectory is low enough that the imaging-based method can be used as a valuable equilibrium reconstruction constraint.

II. PerSpect SIMULATION

A “ground-truth” magnetic field is obtained from MSTFit, a toroidally symmetric two-dimensional (2D) fixed boundary equilibrium reconstruction code. The magnetic field considered herein is that of standard 385 kA MST plasma discharge during a period between sawteeth. Initial conditions of an ion beam including species, position, injection angle, and energy are prescribed. A three-dimensional (3D) ground-truth beam trajectory is then calculated using the initial beam conditions and magnetic field. A method considered by Verlet⁶ was chosen for the trajectory calculation to reduce cumulative errors. The force due to the radial electric field is ignored because it is negligible compared to the $v \times B$ term in the center region of MST (Ref. 7) ($r/a=0.3-0.7$), where the ion beam will be imaged. In this simulation we use a 70 keV sodium beam originating from the port on MST where the HIBP is installed.

We created simulation tools to evaluate the visual field and projected quality of images given a camera located at various ports on the MST. They will help determine suitable camera locations, and are used to model data that would be collected in an actual experiment. This simulation, which we call PerSpect (for perspective view of spectral images), is

^{a)}Electronic mails: chao.ling@emerson.com, connor@ecse.rpi.edu, diane@ecse.rpi.edu, rjradke@ecse.rpi.edu, and schoch@ecse.rpi.edu

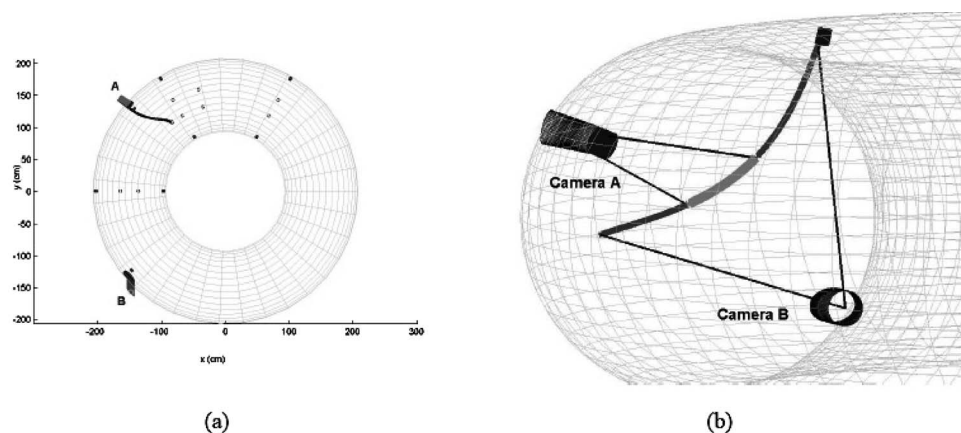


FIG. 1. Top view (a) and closeup (b) of the simulated MST, including ports, transition chambers, cameras, and sample ion beam trajectory. The visual field of each camera is also shown in (b).

implemented in MATLAB. The model is a rendering of the inner and outer walls of MST and includes various landmarks, ports, and transition chambers. The calculated ion beam trajectory is included in this 3D model.

Figure 1(a) shows the top view of the simulated MST torus and the ground-truth primary trajectory. The cameras in the simulation are placed at the ends of two transition chambers (at A and B) extending from MST. Figure 1(b) shows a closeup view of this model with the viewing cones of the cameras superimposed. The major radius of the torus is 150 cm, the minor radius is 52 cm, and the thickness of the torus wall is 5 cm.

A. Trajectory model

Finite ion beam size and beam current density profile were considered when modeling the ion beam trajectory. The ion beam trajectory's cross-section diameter of 1 cm was estimated from HIBP operation on MST as well as accelerator simulation,³ and the beam current density profile is assumed to be Gaussian with 3σ value of 0.5 cm. The current density profile does not affect the simulation results for the purpose of determining the visual field of the camera and the beam location inside the torus. Thus, for these purposes we model the trajectory as a solid tube of 1 cm diameter.

B. Camera model

The cameras are modeled as ideal (pinhole) perspective cameras. Hence, each camera's visual field can be viewed as a cone extending from the camera center, as shown in Fig. 1(b). The portion of the trajectory captured by each camera is the intersection of the trajectory with the cone. We tested two camera locations at the ends of transition chambers attached to ports A and B shown in Fig. 1 at $[\text{poloidal angle}(\theta), \text{toroidal angle}(\phi)] = (19^\circ, 138^\circ)$ and $(-19^\circ, 222^\circ)$, respectively, with the primary ion beam entering MST at $(105^\circ, 128^\circ)$. These ports were chosen because they will give both poloidal and toroidal views of the ion beam trajectory.

C. Transition chamber

The interior portion of MST imaged by a camera is determined by the length and diameter of the transition chamber to which the camera is attached. Cameras cannot be di-

rectly affixed to the outer surface of MST, since exposure to the plasma would damage the optics. In our simulations, we used transition chambers that are 22 cm (on port A) and 15 cm (on port B) long, resulting in solid visual angles of 23° and 44° , respectively.

D. PerSpect simulation evaluation

The simulation shows that camera A can image 25% of the trajectory, while camera B can image 100% of the trajectory, which is 120 cm long. This is the result of the ports chosen and the camera locations. Other ports were investigated, but these offer sufficient coverage and are nearly orthogonal. The image that would be acquired by a camera can be obtained with standard ray-tracing techniques.⁸ That is, the image plane is divided into a grid of pixels, and a ray is cast from the camera center through each pixel location until it intersects an object in the 3D model. We use a gray-scale map to register the objects that the ray encounters, i.e., the transition chamber's inner surface (light gray), the port's inner surface (dark gray), the sample trajectory (black), and the inner wall of the torus (white). Figure 2 shows an example of the 2D images produced with this method.

The PerSpect simulation is quite useful in that it allows us to explore the effects of image resolution, focal length, and camera placement, prior to hardware installation. In the following sections, we process the images in the manner that we plan to process images from real cameras.

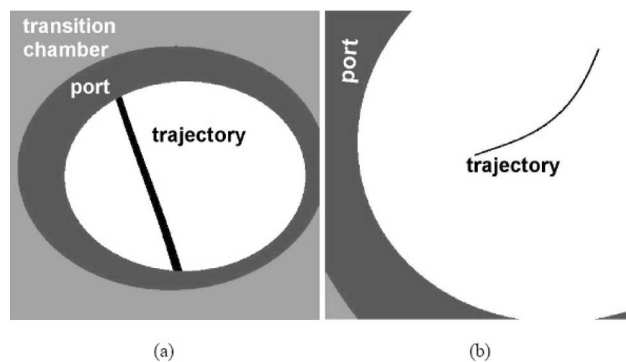


FIG. 2. Ray-traced images of the torus interior from (a) camera A and (b) camera B.

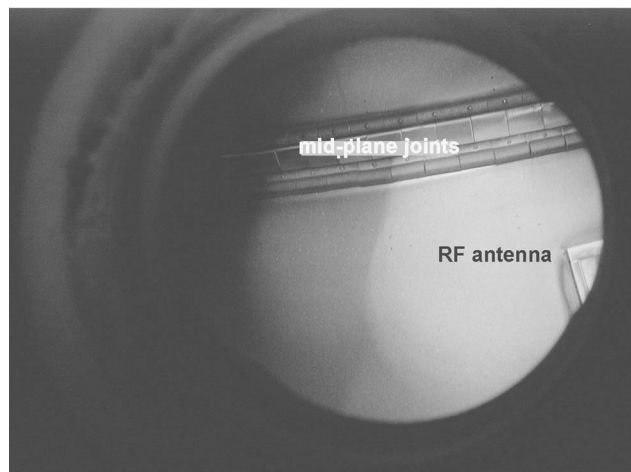


FIG. 3. Port A's view of MST interior landmarks, including the inner mid-plane and a corner of a RF antenna.

III. 3D RECONSTRUCTION OF THE TRAJECTORY FROM TWO 2D IMAGES

A. Sharp images

Given two sharp images of the same trajectory, the original three-dimensional trajectory can be reconstructed if the positions of the cameras are known. Since we will be able to precisely position the cameras on the torus, we expect this information to be available. Additional fine tuning of the camera parameters can be accomplished using the process of camera calibration, which is based on the locations of several features in the cameras' field of view⁹ (in our case, ports, interior midplane, etc.). At least seven features are needed to calibrate the two camera stereosystem in order to reconstruct the 3D scene.¹⁰ Figure 3 shows an actual photograph taken from port A. The inner midplane and one corner of the RF antenna can be clearly seen.

The 3D reconstruction process is based on triangulation. For every pixel in image A determined to lie on the trajectory, a ray R is cast from the center of camera A through this pixel into space. The corresponding trajectory point in image B is obtained by finding the ray from the center of camera B that comes closest to ray R (see Fig. 4). If this distance is below a threshold (i.e., the two rays are suitably close), the point closest to both rays is taken as a 3D trajectory point. In the case of ideal trajectory images (i.e., no noise, infinite resolution), the reconstructed 3D trajectory should coincide

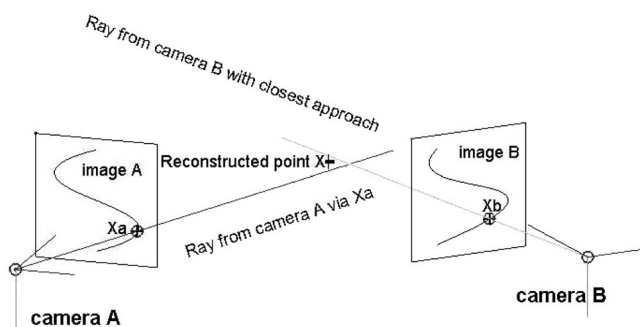


FIG. 4. Triangulation of trajectory points from 2D images.

exactly with the real trajectory (within machine computational error).

B. Realistic images

Detecting which pixels lie on the trajectory of real image pairs is challenging. The images will have noise and the pixel resolution will be finite. It is straightforward to simulate these effects in software and to test the effectiveness of the algorithms on the realistic images. Here, we address modeling of the finite beam size, beam current profile, and background noise. When actual camera data are obtained, additional modeling may be necessary to evaluate the impact of plasma light and other factors.

To simulate the Gaussian intensity profile of the trajectory (which is proportional to the ion beam current density profile), we convolve a Gaussian mask with each projected trajectory image pixel. The size of the mask and its variance (in terms of pixels) are selected such that the simulated trajectory width in each image approximately matches the result of projecting a 1 cm diameter trajectory in 3D onto the corresponding image plane. The apparent width of the trajectory in each image is inversely proportional to the distance from the camera center to the scene, given the same camera focal length and resolution. The ratio of the width of the projected ion beam trajectory on image plane A versus image plane B is approximately 4:1, since camera A is closer to the scene than camera B. The convolved results yield a fuzzy tube with 3σ radius that closely matches the width of the projected 1 cm solid tube from the more accurate ray-traced images. We also added zero mean white Gaussian noise with variance of 0.0025 (the image intensities are in the range of [0,1]) to the image before 3D trajectory reconstruction. Noise is expected in images taken with real cameras due to various sources such as background plasma noise, electronic components, and cosmic rays.

Using the simulated ion beam images, we next detect trajectory points from these noisy images by adapting a robust centerline-tracing algorithm originally developed for segmenting blood vessels in the retina.¹¹ The estimated centerline points can then be interpolated with a smooth curve, (e.g., a spline^{12,13}). The results of the tracing process for noisy images are illustrated in Figs. 5(a) and 5(b), showing that the centerlines are accurately estimated in each image of the trajectory. Finally, the triangulation procedure discussed previously was applied to the spline-interpolated centerline images and the 3D trajectory reconstructed [Fig. 5(c)]. In places where both cameras image the same trajectory portion, the reconstruction matches with the ground-truth trajectory with mean distance between each reconstructed point and the original trajectory equal to $\mu=0.09$ cm.

Error analysis of 3D reconstruction

The reconstructed 3D trajectory is slightly inaccurate due to errors in estimating positions of the centerline points in the 2D images. The 3D reconstruction error due to noise in projected points from two cameras was addressed by Rodrigues and Aggarwal.¹⁴ We approximate the noise in each 2D trajectory pixel as independent and identically distributed

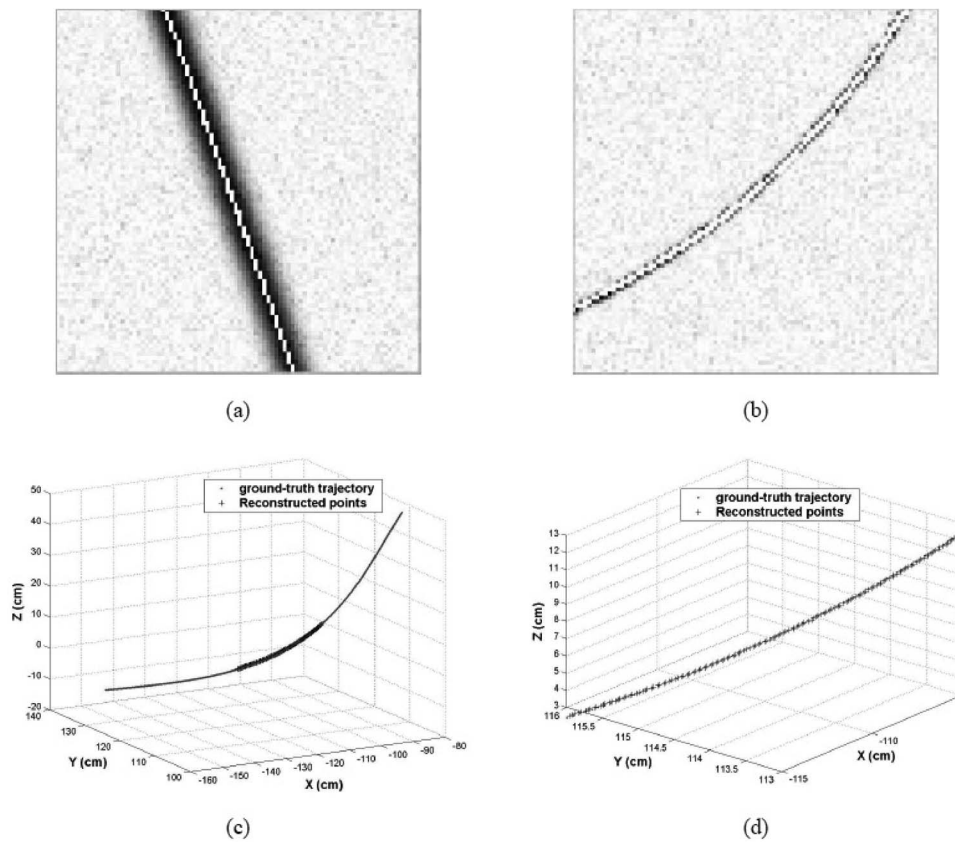


FIG. 5. 3D reconstruction of a sample primary trajectory based on two noisy images. [(a) and (b)] Original projected images from cameras A and B, respectively, superimposed with estimated trajectory centerlines obtained from the tracing algorithm. (c) The section of the reconstructed 3D trajectory. The reconstruction matches with the true trajectory with $\mu=0.09$ cm after spline interpolation. (d) A closeup of the reconstructed trajectory.

with normal distribution of zero mean and known covariance matrix (here, the 2×2 identity matrix). The triangulation method used here is equivalent to minimizing the average distance between each measured image point and its estimated projection.

At each estimated 3D trajectory point, we can illustrate the uncertainty in its position as an ellipsoid whose axes are aligned with the eigenvectors of the 3D covariance matrix of its error. The length of each axis is visualized as three times the corresponding eigenvalue (Fig. 6). The uncertainty ellipsoids are skinny perpendicular to the central axis of camera A (which is near the trajectory) and thicker perpendicular to the central axis of camera B (which is farther away). This sensitivity analysis naturally confirms that the estimated location of the reconstructed point is more sensitive to the camera that is farther from the scene.

IV. THE RECONSTRUCTED ION BEAM TRAJECTORY USED AS A CONSTRAINT IN MSTFit

The reconstructed 3D ion beam trajectory may provide an additional magnetic equilibrium reconstruction constraint. The local curvature of the trajectory can give the component of the magnetic field that is perpendicular to the ion trajectory; however, no direct information is obtained for the component of the B field that is parallel to the ion trajectory. To demonstrate the usefulness of the ion beam imaging system, the equilibrium reconstruction code MSTFit was used to generate several equilibria with distinct internal features and identical edge values. Ion trajectories were calculated for each of these as a way to discern if the beam motion in a plasma is sensitive to the difference in the magnetic field.

FIG. 6. 3σ isoprobability ellipsoid plot around a sample reconstructed point. The radii of the ellipsoid are 0.26, 0.26, and 1.24 cm.

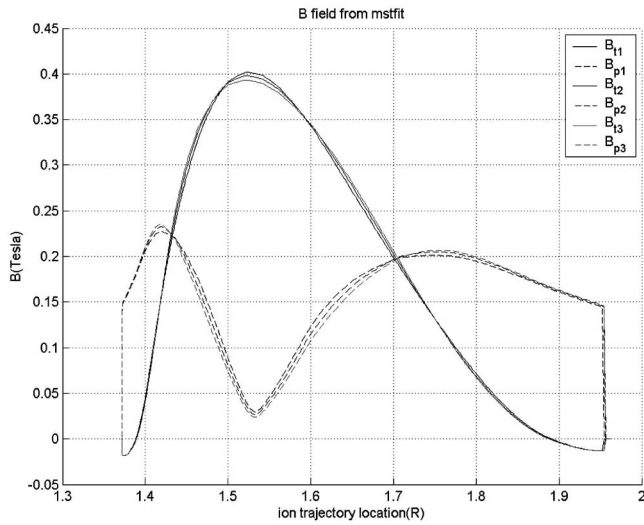


FIG. 7. Three B field equilibria produced by MSTFit corresponding to an on-axis value of $q=0.17, 0.19,$ and 0.21 .

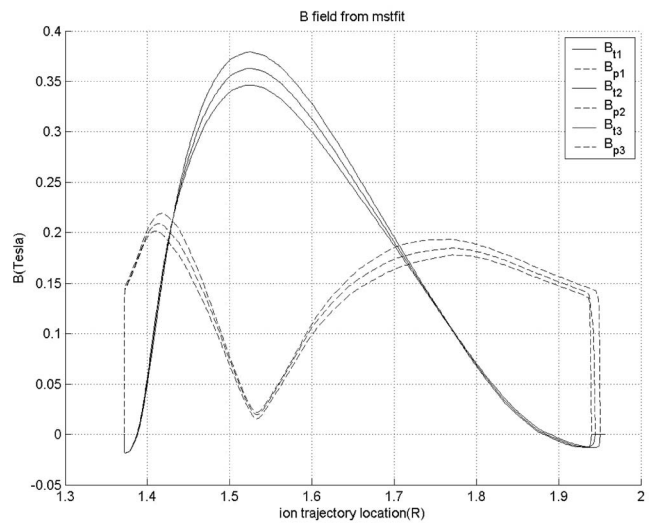


FIG. 8. Three B field equilibria produced by MSTFit corresponding to a different central value of $B_0=0.32, 0.34,$ and 0.36 T.

MSTFit determines the equilibria by finding the solution to the Grad-Shafranov equation that best fits experimental data. The best fit is determined by minimizing a weighted χ^2 cost function that incorporates data from several diagnostics, including HIBP trajectories. The B field grid resolution used is 2×2 cm², and interpolation is used to calculate the magnetic field between grid points.

The prescribed B field was produced by MSTFit for a standard 385 kA plasma discharge during a time between sawteeth. Three magnetic reconstructions were created using different constraints; specifically, q on axis were constrained to be 0.17, 0.19, and 0.21. The toroidal (B_t) and poloidal (B_p) components of the magnetic field for these three fits are plotted in Fig. 7. In this case, we can see that the magnetic field profiles did not change as much as the current profiles. Another three reconstructions were generated with q on axis fixed, but the B on axis were constrained to be 0.32, 0.34, and 0.36 T. These are plotted in Fig. 8. Ion trajectories using the image-based reconstruction method were calculated for

the six magnetic reconstructions shown in Figs. 7 and 8. These are shown in Figs. 9 and 10, respectively.

It is seen that the equilibrium profiles with different on-axis B fields generate trajectory loci that are statistically different, i.e., the distance between the outer two trajectories and the center one are larger than the 3σ isoprobability error ellipsoid for each trajectory point. However, the three trajectories with different on-axis q are not distinguishable from each other; they are all within the 3σ isoprobability error ellipsoid. The radii of the middle ellipsoid for these two sets of equilibria are 0.26, 0.26, and 1.24 cm and 0.30, 0.31, and 1.19 cm, respectively. The beam imaging technique appears to be more sensitive to the magnitude of the on-axis B field than to the central q value.

V. CONCLUSIONS

The spectroscopic imaging technique has shown satisfactory results on a simulation level. The simulations and analysis software will aid in hardware selection and experi-

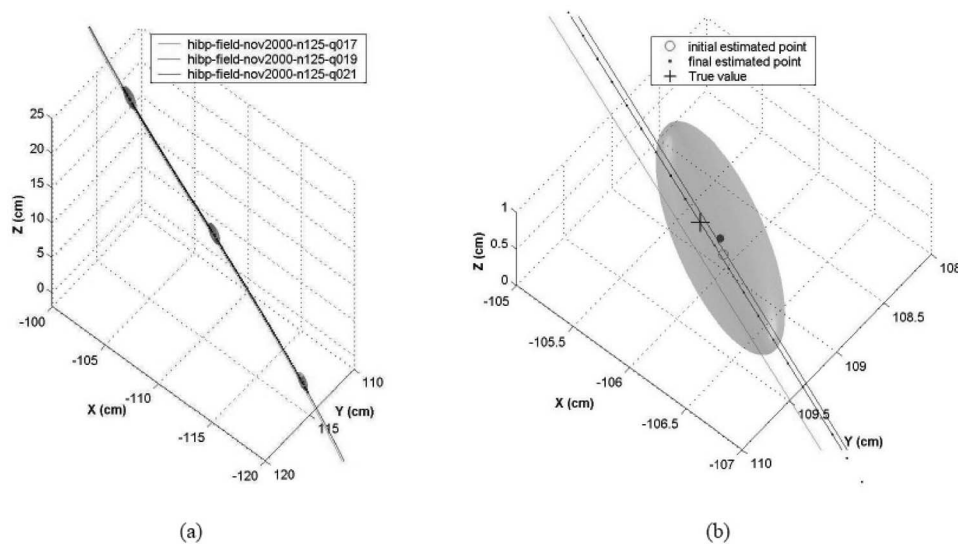


FIG. 9. (a) Covariance ellipsoid 3σ plot and three trajectories corresponding to three magnetic equilibria produced by MSTFit for on-axis q values of 0.017, 0.019, and 0.021. (b) A closeup of the middle point; the radii of the middle ellipsoid are 0.30, 0.31, and 1.19 cm.

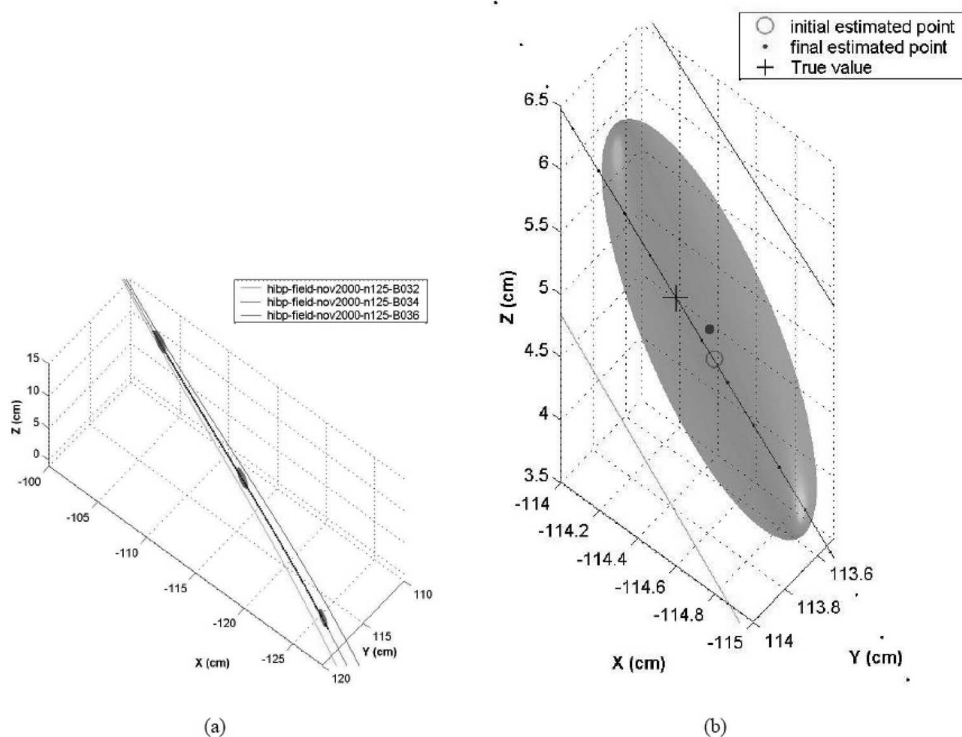


FIG. 10. (a) Covariance ellipsoid 3σ plot and three trajectories corresponding to three magnetic equilibria produced by MSTFIT with on-axis B values of 0.32, 0.34, and 0.36 T. (b) A close-up of the middle point; the radii of the middle ellipsoid are 0.26, 0.26, and 1.24 cm.

mental setup and will be used to process experimental data when it is available. Issues of finite beam size, background noise, pixelization, and camera location have been studied. Error analysis of the 3D reconstructed trajectory shows that the 3D point positions are more sensitive to the trajectory's image in the more distant camera. The accuracy of the reconstructed 3D trajectory points will ultimately depend on factors such as the image resolution, background noise, and camera calibration.

Calculations using magnetic fields produced with MSTFit show that heavy ion beam trajectories may help distinguish magnetic fields from plasmas with similar equilibria, and thus this beam imaging technique may provide useful constraints for equilibrium reconstructions with MSTFit.

ACKNOWLEDGMENTS

The authors would like to thank Dr. J. K. Anderson for his insightful discussions and provision of MSTFit equilibrium reconstruction code support. This work is supported by the U.S. Department of Energy.

- ¹F. C. Jobses and M. Peng, APS Meeting Abstracts, 1997, p. 316.
- ²D. R. Demers, P. M. Schoch, R. J. Radke, J. K. Anderson, D. Craig, and D. J. Den Hartog, *Rev. Sci. Instrum.* **74**, 2103 (2003).
- ³D. R. Demers, K. A. Connor, P. M. Schoch, R. J. Radke, J. K. Anderson, D. Craig, and D. J. Den Hartog, *Rev. Sci. Instrum.* **75**, 4187 (2004).
- ⁴J. Lei, *Rev. Sci. Instrum.* **70**, 967 (1999).
- ⁵J. K. Anderson, *Nucl. Fusion* **44**, 162 (2004).
- ⁶L. Verlet, *Phys. Rev.* **159**, 98 (1967).
- ⁷U. Shah, Ph.D. thesis, Rensselaer Polytechnic Institute, 2001.
- ⁸A. Fujimoto, T. Tanaka, and K. Iwata, *IEEE Comput. Graphics Appl.* **6**, 16 (1986).
- ⁹R. I. Hartley and A. Zisserman, *Multiple View Geometry in Computer Vision*, 2nd ed. (Cambridge University Press, Cambridge, 2004).
- ¹⁰G. Xu and Z. Zhang, *Epipolar Geometry in Stereo, Motion, and Object Recognition: A Unified Approach* (Kluwer Academic, Norwell, 1996).
- ¹¹A. Can, H. Shen, J. N. Turner, H. L. Tanenbaum, and B. Roysam, *IEEE Comput. Graphics Appl.* **3**, 125 (1999).
- ¹²G. Farin, *Curves and Surfaces for Computer-Aided Geometric Design: A Practical Guide*, 4th ed. (Academic Press, Boston, MA, 1997).
- ¹³I. Lee, *Comput. Aided Geom. Des.* **17**, 161 (2000).
- ¹⁴J. J. Rodriguez and J. K. Aggarwal, *Proceeding of IEEE Computer Society Conference on Computer Vision and Pattern Recognition*, 1988, pp. 153–158.